Global Characteristics of Observable Foreshocks for Large Earthquakes

Nadav Wetzler*1[©], Thorne Lay², and Emily E. Brodsky²

Abstract

Foreshocks are the only currently widely identified precursory seismic behavior, yet their utility and even identifiability are problematic, in part because of extreme variation in behavior. Here, we establish some global trends that help identify the expected frequency of foreshocks as well the type of earthquake most prone to foreshocks. We establish these tendencies using the global earthquake catalog of the U.S. Geological Survey National Earthquake Information Center with a completeness level of magnitude 5 and mainshocks with $M_{\rm w} \ge 7.0$. Foreshocks are identified using three clustering algorithms to address the challenge of distinguishing foreshocks from background activity. The methods give a range of 15%-43% of large mainshocks having at least one foreshock but a narrower range of 13%-26% having at least one foreshock with magnitude within two units of the mainshock magnitude. These observed global foreshock rates are similar to regional values for a completeness level of magnitude 3 using the same detection conditions. The foreshock sequences have distinctive characteristics with the global composite population b-values being lower for foreshocks than for aftershocks, an attribute that is also manifested in synthetic catalogs computed by epidemic-type aftershock sequences, which intrinsically involves only cascading processes. Focal mechanism similarity of foreshocks relative to mainshocks is more pronounced than for aftershocks. Despite these distinguishing characteristics of foreshock sequences, the conditions that promote high foreshock productivity are similar to those that promote high aftershock productivity. For instance, a modestly higher percentage of interplate mainshocks have foreshocks than intraplate mainshocks, and reverse faulting events slightly more commonly have foreshocks than normal or strike-slip-faulting mainshocks. The western circum-Pacific is prone to having slightly more foreshock activity than the eastern circum-Pacific.

Cite this article as Wetzler, N., T. Lay, and E. E. Brodsky (2023). Global Characteristics of Observable Foreshocks for Large Earthquakes, *Seismol. Res. Lett.* **94**, 2313–2325, doi: 10.1785/0220220397.

Supplemental Material

Introduction

Foreshock sequences have long been documented at a global scale. The relatively high magnitude of completeness ($M_c \sim 5$) for global catalogs requires considering a minimum magnitude threshold for mainshocks of ~ 6.5 –7 (e.g., Jones and Molnar, 1979; von Seggern *et al.*, 1981; Reasenberg, 1999; Marsan *et al.*, 2014; Wetzler *et al.*, 2017), making the task of sparse foreshock identification difficult, especially for regions with low seismicity rates (Reasenberg, 1999). However, with the progressive accumulation of large earthquakes and their accompanying foreshocks sequences, the statistical significance of foreshock occurrence characteristics for $M_c = 5$ can now be better established.

Previous studies at a global scale have identified some common features of foreshock sequences. One of the fundamental observations is that the seismicity rate sometimes increases relative to the background activity within days to weeks prior to the mainshock (Jones and Molnar, 1979; von Seggern *et al.*, 1981). Seismicity rates of stacked foreshock sequences show

inverse-Omori law patterns with accelerated rates approaching the mainshock (Kagan and Knopoff, 1978; Yabe and Ide, 2018), as is also found for epidemic-type aftershock sequence (ETAS) models, albeit with lower power law than for aftershocks (Helmstetter *et al.*, 2003). This allows space–time clustering to be used to isolate foreshock sequences, even for global catalogs with relatively high M_c . However, the percentage of mainshocks with observed foreshocks on global levels is quite low with estimates of 10% (Jones and Molnar, 1979), 16.5% (Reasenberg, 1999), and 20% (von Seggern *et al.*, 1981). These low levels contrast with some regional studies that have proposed foreshock rates as high as ~75% when small earthquakes

^{1.} Geological Survey of Israel, Jerusalem, Israel, https://orcid.org/0000-0002-7552-0866 (NW); 2. Department of Earth and Planetary Sciences, University of California Santa Cruz, Santa Cruz, California, U.S.A., https://orcid.org/0000-0003-2360-4213 (TL); https://orcid.org/0000-0002-6855-6860 (EEB)

^{*} Corresponding author: nadavw@gsi.gov.il

[©] Seismological Society of America

can be detected and M_c is much lower (Trugman and Ross, 2019). However, these high foreshock levels were revisited by van den Ende and Ampuero (2020), and Moutote *et al.* (2021), who obtain lower estimates when considering time varying background seismicity and cascading processes.

Previous studies have also suggested that foreshocks can be viewed as mainshocks that happen to have larger aftershocks, suggesting no physical difference between foreshocks and aftershocks (Felzer et al., 2004). However, spatial variations of foreshock occurrence have been observed at a global scale. Mainshocks along the east Pacific rise transform faults were documented to have higher probability of having foreshock sequences compared with continental transform faults (McGuire et al., 2005). Aftershock distribution and faulting geometry may be affected by mechanical conditions and transient stress changes at the periphery of the mainshock (Hasegawa et al., 2012; Wetzler et al., 2017, 2018). Correspondingly, foreshocks tend to have distribution and faulting geometry affiliated with the mainshock nucleation (e.g., Wetzler et al., 2017) and a general similarity of the faulting geometry among the foreshocks (Jones and Molnar, 1979). This global tendency is documented by Wilding and Ross (2022), who show that foreshock activity has more similar moment tensors to the mainshock compared with aftershock activity.

In addition, a precursory migration toward the mainshock hypocenter has been observed prior to some large ruptures, as in the case of the 2011 Tohoku, Japan, and 2014 Iquique, Chile, events (e.g., Kato and Igarashi, 2012; Brodsky and Lay, 2014; Ruiz *et al.*, 2014). It has also been proposed that thrust mainshocks have larger tendency for foreshock occurrence compared with strike-slip mainshocks (Reasenberg, 1999).

Although most of the previous global studies of foreshocks have used fixed spatial and time windows for capturing any seismicity changes before the mainshocks, we revisit the foreshock behavior in an updated global catalog using several techniques for foreshock cluster recognition that have been applied on regional scales using catalogs with lower M_c (e.g., Wetzler et al., 2022). This includes methods for reducing background activity contributions. We exploit the availability of focal mechanism solutions for most of the events considered to examine influences of tectonic regime on foreshock occurrence.

Dataset

We use the global U.S. Geological Survey National Earthquake Information Center (NEIC; see Data and Resources) earthquake catalog (Fig. 1; Masse and Needham, 1989) for shallow depth (\leq 70 km) events from 1 January 1976 to 1 January 2020. A magnitude of completeness ($M_c = 5.0$) and b-value (1.06) for the NEIC catalog (Fig. S1, available in the supplemental material to this article) are defined from the goodness of fit using a Kolmogorov–Smirnov (K–S) test with a smoothing constraint between observed and theoretical Gutenberg–Richter distributions from maximum-likelihood estimation for a range of

considered $M_{\rm c}$ levels (e.g., Goebel *et al.*, 2017). We remove all events with magnitudes <5.0. The total number of earth-quakes remaining is 57,591, with 463 having $M_{\rm w} \ge 7.0$. We also consider focal mechanisms of corresponding earthquakes from the Global Centroid Moment Tensor (Global CMT) catalog (Dziewoński *et al.*, 1981; Ekström *et al.*, 2012; see Data and Resources).

Earthquake Clusters

Earthquake sequences are identified in the $M \ge 5.0$ NEIC global catalog using the three clustering methods described by Wetzler et al. (2022). The first method is a nearest-neighborhood algorithm (ZnBZ) developed by Zaliapin and Ben-Zion (2013) using the metric proposed by Baiesi and Paczuski (2004). The NEIC catalog shows clear separation between background and clustered seismicity in ZnBZ rescaled space and rescaled time for event pairs (Fig. S2). The position of the line separating clustered and background is based on comparison with reshuffled catalog without spatial-temporal seismicity clustering, in which the separation threshold is determined from the 99th percentile of 100 random catalog representations, as described by Wetzler et al. (2022). The clustered activity in the lower left portion of the plot represents 30% of the catalog, and the decision line for excluding background events is well defined. The second clustering method is a magnitude-varying space + fixed-time windowing procedure (WnC), by which earthquakes are grouped to clusters with a fixed foreshock time window of 30 days prior to the mainshock and an aftershock window 60 days after the mainshock. The spatial window is based on a mainshock magnitude dependent radius R given by

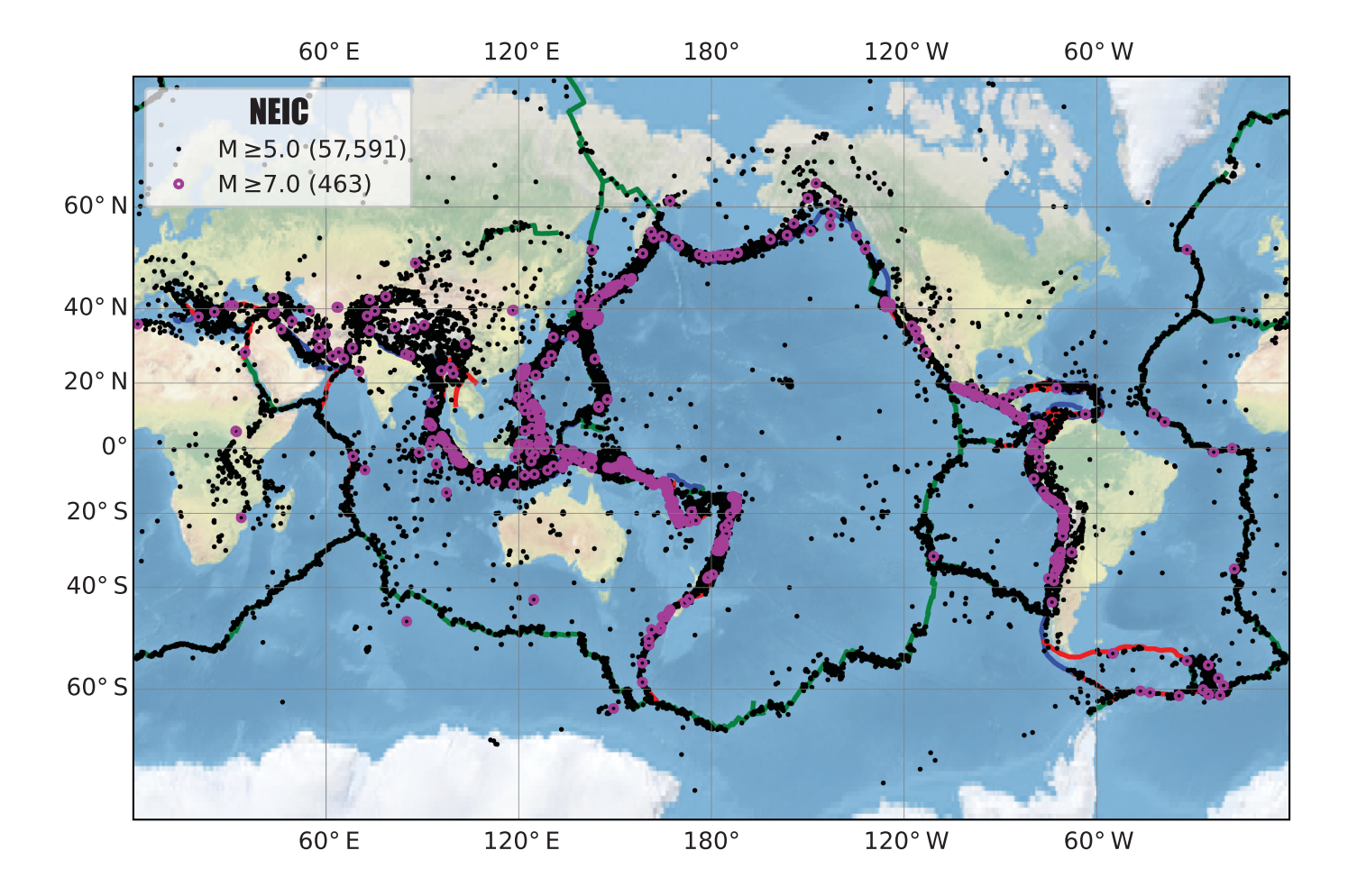
$$R = L_{\text{WnC}} \times q,$$

$$q = \{1.0, \text{if } M \ge 9; 1.5, \text{if } 8 \le M < 9; 2.0, \text{if } M < 8\},$$
(1)

in which $L_{\rm WnC}$ is the rupture length estimated by Wells and Coppersmith (1994), adjusted by q to account for the rupture lengths of some huge megathrust earthquakes. The third clustering procedure, the time magnitude clustering (TMC) method, defines clusters using a linkage algorithm prescribed by magnitude-dependent spatial and temporal distances following the widely used Gardner and Knopoff (1974) approach with modified conditions representing the triggering distances between earthquake pairs. The spatial condition is similar to the WnC method for each event with magnitude M, without the amplification of q parameter (equation 1), and the temporal triggering window is defined by

$$t = 0.1e^M, (2)$$

in which t is the time window (in days). Figure S3 shows comparisons of the dimensions of the time and spatial windows of TMC, WnC, and Gardner and Knopoff (1974).



Mainshocks

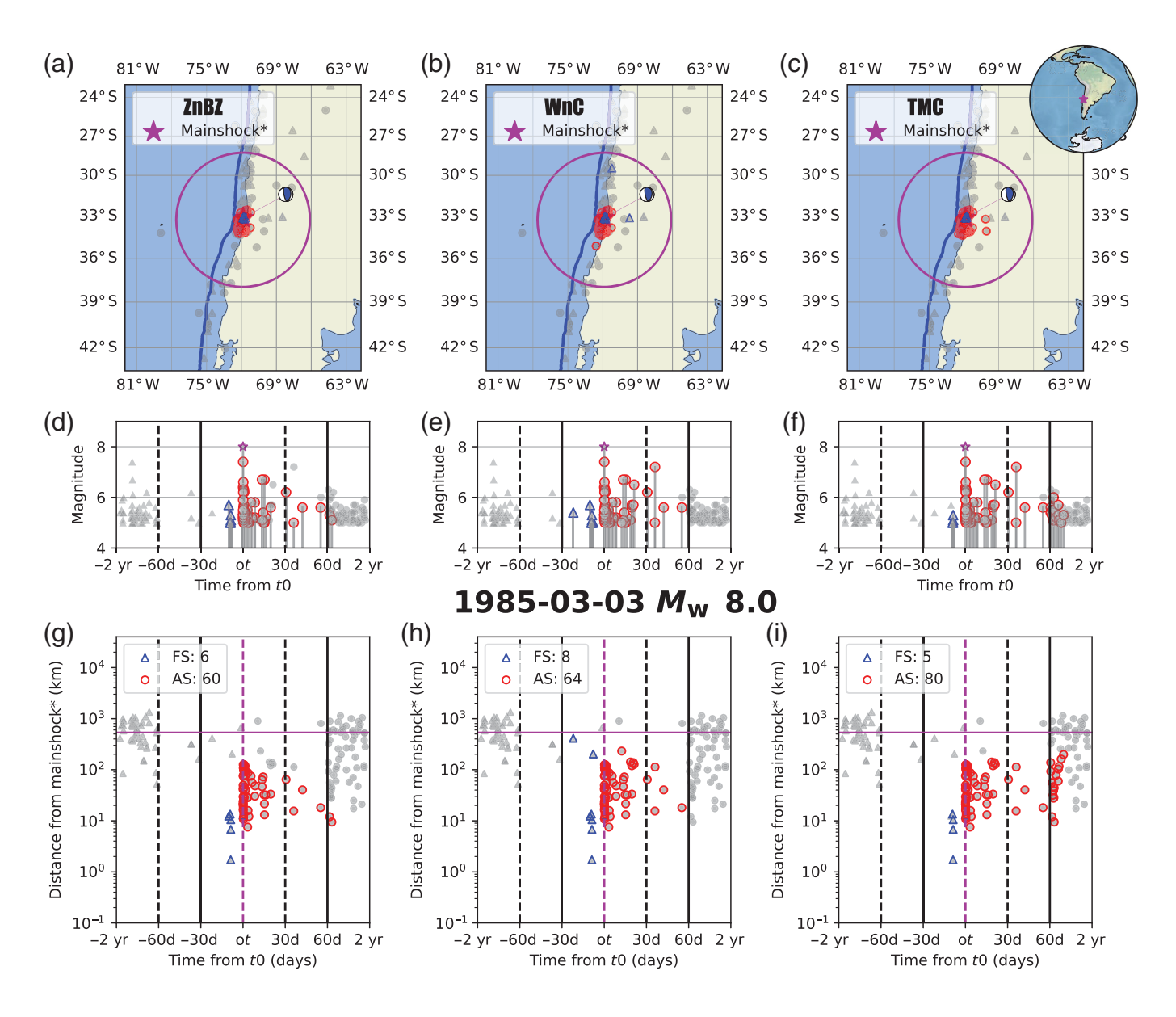
For each earthquake cluster, mainshocks are considered to be the earthquake with the largest magnitude. To reduce the effect of overestimation of foreshock counts due to sequential large magnitude sequences, we retain typical mainshock-aftershock sequences, with aperture of at least 0.5 magnitude units between the mainshock and the second largest earthquake in each cluster. This excludes sequences that can be characterized as doublets (e.g., Lay and Kanamori, 1980), triplets, or swarms, for which defining foreshocks is ambiguous, but allows for the large range in Båth's law parameter (Båth, 1965) observed among events. In addition, we only consider mainshocks with $M_{\rm w} \ge 7.0$, a minimum of 2.0 units above our uniform M_c , and with a total number of ≥ 4 events in a cluster apart from the mainshock (labeled here as mainshock*). Further discussion of the decision scheme is presented by Wetzler et al. (2022).

The total number of detected clustered sequences are 379 for the ZnBZ method, 356 for the WnC method, and 357 for the TMC method. These numbers decrease by 19% (ZnBZ), 26% (WnC), and 14% (TMC), when we consider only clusters with a minimum of four events (Fig. S4). The percentage of all clusters represented by mainshock* sequences ranges between 89% for the ZnBZ and WnC methods and 85% for the TMC case (Fig. S4). The classification of other cluster types

Figure 1. Seismicity map for the National Earthquake Information Center (NEIC) global earthquake catalog from 1976 to 2020 for events with $M \ge 5.0$ (black dots) and major events with $M_{\rm w} \ge 7$ (magenta circles). Plate boundaries are plotted following Bird (2003): transforms (red), trenches (blue), and ridges (green).

(doublets, triplets, and swarms) is similar for all three clustering algorithms, and these sequences are excluded.

We classify the mainshock faulting geometry using focal mechanisms obtained from the Global CMT catalog and the method described by Shearer et al. (2006). The method converts the rakes of the two nodal planes to a single value ranging from -1 to 1, in which normal faulting has values from -1 to -0.5, reverse faulting has values from 0.5 to 1.0, and zero (±0.25) is strike-slip faulting. To focus on the end-member faulting geometries, we also consider oblique faulting between −0.5 to −0.25 and 0.25 to 0.5. Interplate events are designated by the geographic proximity to a similar orientation plate boundary type (Bird, 2003) at a maximum distance defined by the WnC effective radius (see Fig. 2). Mainshocks that do not share similar faulting geometry with the plate boundary are located beyond a rupture length from plate boundaries or are defined as oblique faulting are designated as intraplate events.



Foreshock Comparisons Between Methods

Foreshock occurrences at a global scale

Foreshocks for the NEIC catalog with $M \ge 5$ are identified by the three clustering algorithms for all events labeled as mainshocks*. The three methods provide comparable counts of foreshocks and aftershocks in some cases. An example is shown for the 3 March 1985 $M_{\rm w}$ 8.0 Chile megathrust earthquake (Fig. 2), with results consistent with the foreshock estimate in a previous study (Choy and Dewey, 1988). In this case, the three algorithms give similar foreshocks counts (5–8), with all events occurring within the 30-day time window of the WnC method. The WnC method captures two somewhat isolated events at large distance within the time window that may or may not be background activity, and this counting of all events in the window tends to give higher foreshock counts for this method overall (Fig. 3a). Comparisons between the methods for all individual sequences are available in Figure Bundle 1 in the supplemental material

Figure 2. Example comparison between the three clustering methods for the 3 March 1985 $M_{\rm w}$ 8.0 Chile (interplate mainshock*) for the NEIC global catalog. The upper rows show map views of the seismicity ($M \ge 5.0$) with background events (gray) that occurred prior to the mainshock (triangles) or after (circles) as were detected by the (a) ZnBZ, (b) WnC, and (c) TMC methods. The identified foreshocks are plotted in blue (triangles) and aftershocks in red (circles). The magenta circles represent the effective radius of the mainshock (equation 1). Focal mechanism solution of the mainshock is from the Global Centroid Moment Tensor (Global CMT) catalog. Timelines with nonlinear scale are shown for the seismicity in each map versus magnitude as were detected by the (d) ZnBZ, (e) WnC, and (f) TMC methods. Timelines with nonlinear scale are shown for seismicity epicentral distances from the mainshock* for (g) ZnBZ, (h) WnC, and (i) TMC clustering methods with the same color scheme. A global map with the mainshock* location (magenta star) is inserted above (c).

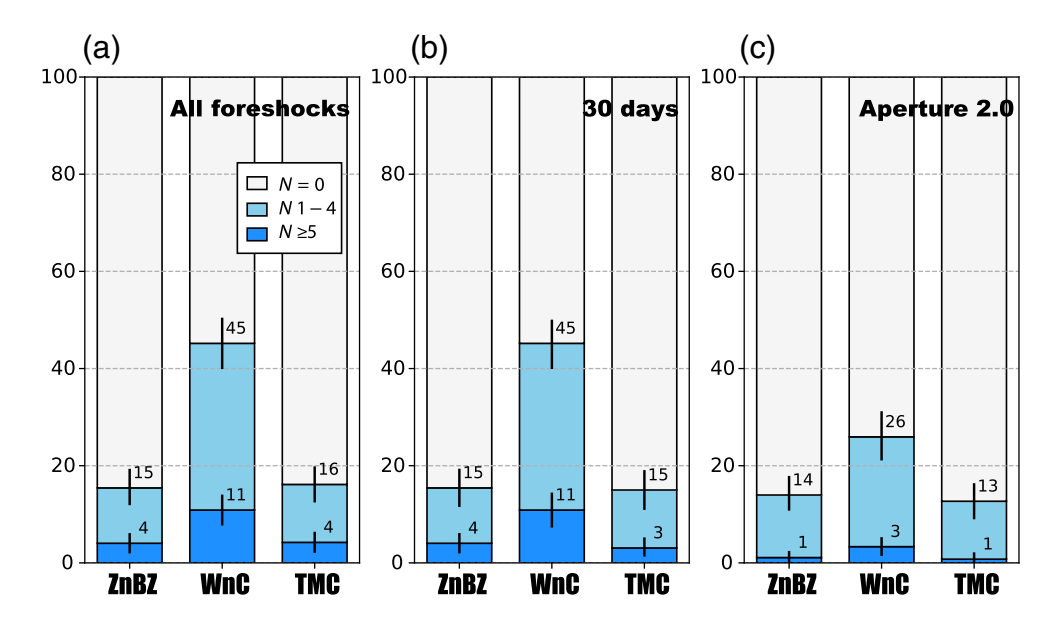


Figure 3. The percentage of mainshock* events with observable foreshocks (colored portions of histograms; dark blue indicates that the number of foreshocks is ≥5, light blue indicates that the number of foreshocks is from 1 to 4); the white portion indicates events without foreshocks for the NEIC global catalog. This is for all earthquakes above the uniform completeness magnitude, $M_{\rm c} = 5.0$. Results are shown for the three clustering methods: the nearest-neighbor linking (ZnBZ), the magnitude-dependent spatial and 30-day temporal windowing (WnC), and the time and distance magnitude-dependent linking method (TMC). The number of foreshocks is determined for three cases: (a) using all foreshocks in each individual cluster, (b) imposing a constant 30-day foreshock time window, and (c) considering only earthquakes within 2.0 magnitude units below the mainshock magnitude. The black vertical lines represent the 5% and 95% confidence level of 500 bootstrap random realizations of the populations. The color version of this figure is available only in the electronic edition.

(see Data and Resources). The ZnBZ and the TMC methods find 15%–16% of mainshocks with at least one foreshock, whereas the WnC method gives 45% (Fig. 3a). Imposing a fixed time window of 30 days for foreshock sequences for all three methods (Fig. 3b) shows similar counts, highlighting that the large majority of the foreshock sequences occur within 30 days (equation 2).

One strategy to reduce the scatter between methods is to impose a fixed aperture of foreshocks having ≤2 magnitude units below the mainshock value, which results in more similar measurements between methods (Fig. 3c). This restriction gives from 13% to 26% (with average of 18% across all three methods; Table S1) of mainshock* events having observed foreshocks within the specified aperture. These average estimates are the most reliable and are comparable to prior estimates of 10%–20% (Jones and Molnar, 1979; Reasenberg, 1999; von Seggern et al., 1981). The average global NEIC foreshock percentage of ~18% is comparable with regional foreshock observations (Wetzler et al., 2022) for seismogenic areas adjacent to large subduction zones (24% average for Costa Rica, Japan, Greece, and Alaska; see Table S1).

The similarity in the percentages of the TMC and ZnBZ methods compared with the higher value of the WnC method suggests that there is some bias toward higher foreshock

detection due to counting background events in the WnC approach. This highlights the advantage of the triggering based clustering algorithms, but no method is optimal, especially given a relatively high $M_{\rm c}$ catalog.

To demonstrate the robustness of the foreshock seismicity with respect to the background, we compute the ratios between the foreshock and aftershock rates to the background rates in declustered catalogs from each method (Fig. S5). All three methods indicate that the foreshock rates and aftershock rates for most cases (>94%) are above the background rates. This is probably due to the relatively completeness high $(M_c = 5)$ of the global catalog, with relatively low background rates for events of this size.

b-Value

We calculate *b*-values and the corresponding magnitude of completeness for the entire

composite population of foreshocks identified by the ZnBZ method for the NEIC catalog and then for the composite population of ZnBZ identified aftershocks in the catalog (Fig. 4a). The magnitude of completeness and b-values are calculated using the K-S test, with a magnitude bin size of 0.1, yielding a consistent completeness magnitude, $M_c = 5.2$, for both foreshocks and aftershock sequences. The power law b-value slope for the complete foreshock population is lower by 0.44 units than for the aftershock population, compatible with estimates by Gulia and Wiemer (2019) in general, Tamaribuchi et al. (2018) for Japan, and Wetzler et al. (2022) for eight regional catalogs with unified $M_c = 3.0$. Variations in *b*-value estimates are tested for a range of M_c levels (5.0 \leq M_c \leq 6.5), showing that for almost the entire tested range, the b-values of the composite aftershocks are consistently higher than for the foreshocks (Fig. 4c). We repeat the b-value measurement including only foreshocks that occurred between the largest foreshock and the origin time of the mainshock, essentially assuming that the foreshock sequence has mainshock-like distribution internally, as discussed by Wetzler et al. (2022). For this case, b-values of composite foreshock and aftershock sequences are similar (\sim 1.1). However, the *b*-value of the composite foreshocks is unstable for a large range of M_c levels >5.7 (Fig. 4d),

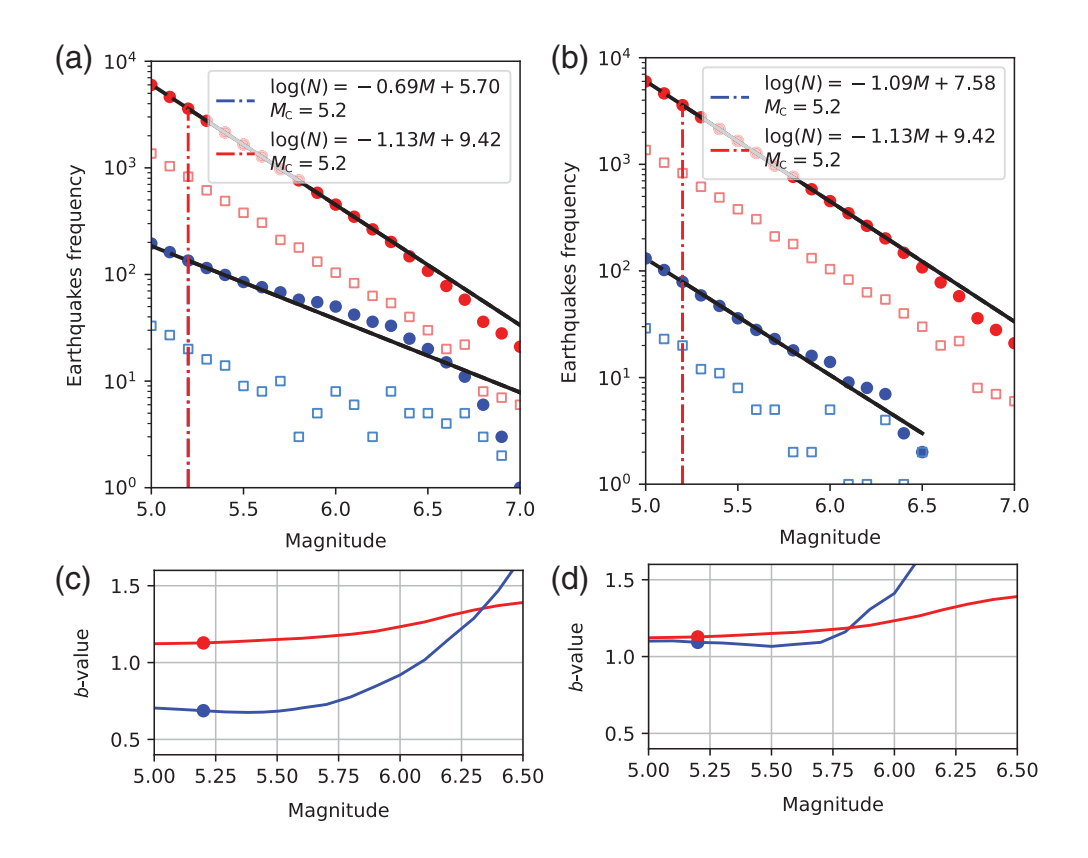


Figure 4. Magnitude distributions (open symbols) and cumulative magnitude distributions (Gutenberg–Richter) relationships (filled symbols) for composite sequences of events labeled as aftershocks (red) and foreshocks (blue) for the NEIC catalog processed with the ZnBZ clustering algorithm. The composite foreshock count is made (a) for the entire labeled foreshock sequence for all mainshocks and (b) for only the foreshocks between the largest foreshock and the mainshock. The maximum-likelihood Gutenberg–Richter distributions for the *b*-value estimates are indicated by the black lines, and values are given in the insets. Variations in *b*-value estimates of foreshocks (blue lines) and aftershocks (red lines) as a function of assumed M_c level using the ZnBZ clustering method are shown in the lower panels (c) for all foreshocks and (d) for foreshocks between the largest foreshock and the mainshock. The best fit M_c levels and *b*-values (dots) are defined by the K–S test.

suggesting a low robustness. Results for the three clustering methods are generally consistent, with b-values lower than for aftershocks (by 0.24 (WnC) to 0.42 (TMC)) when all foreshocks are considered and b-values increasing to near the values for aftershocks when considering only foreshocks between the largest foreshocks and the mainshocks (Fig. S6).

We test the results of the b-value analysis using an ETAS algorithm developed by Mizrahi $et\ al.$ (2021). We use the NEIC catalog from the region of Sumatra (Fig. S7) to invert for the regional ETAS parameters (Fig. S7), assuming the productivity coefficient, $\alpha=1\sim b$, based on the global catalog study of Dascher-Cousineau $et\ al.$ (2020). The inverted parameters are then used to generate a synthetic catalog for the region (Fig. S7b), which was processed by the three clustering algorithms. We calculated the b-value for the composite aftershocks and foreshocks for the two cases (entire foreshock sequence, and from the largest foreshock to the mainshock; Fig. S8). The b-values for composite ETAS foreshock populations are consistently

lower than for aftershocks (by 0.07-0.20 units), which is similar in sign but less pronounced than for the similarly processed NEIC data shown in Figure 4 and Figure S6. When considering only foreshocks after the largest foreshock, b-values for foreshocks increase in all cases, with the ZnBZ and TMC results now having smaller differences between foreshocks and aftershocks (0.06-0.08 units); the sparser result for the WnC algorithm gives a higher, unstable *b*value for foreshocks than for aftershocks. This ETAS comparison thus approximates the observed b-value trends in sign but does not perfectly match them in strength. Similar tendencies were found for ETAS calculations using a different algorithm for $M_c = 5$, and in numerical tests, we found that the specific magnitude-dependent spatial parameters of the clustering algorithms tend to interact with the assumed spatial dependence in the ETAS algorithm to generally cause lower b-value estimates for foreshocks. Using simple temporal windowing, ignoring spatial windows, tends to recover b-values for

foreshocks and aftershocks that are almost the same and match the input b-values. We observed corresponding behavior in our previous analysis of regional ETAS sequences with $M_{\rm c}=3.2$ (Wetzler *et al.*, 2022; Fig. S7).

Foreshocks and mainshock faulting style

We compare foreshock activity for interplate and intraplate mainshocks*, designated by the criteria discussed earlier. We find that for the three clustering algorithms, interplate faulting is consistently more likely to have a few percent higher foreshock occurrence (Fig. 5a). Similar results are obtained when imposing a fixed 30-day time window on all methods (Fig. 5b) and when including only foreshocks that are >2 magnitude units below the mainshock (Fig. 5c). One possible explanation for this observation stems from the concepts of Mogi (1963), which suggest that foreshock activity increases with heterogeneity of the source region stress field. Mature, large cumulative displacement interplate faults may have more

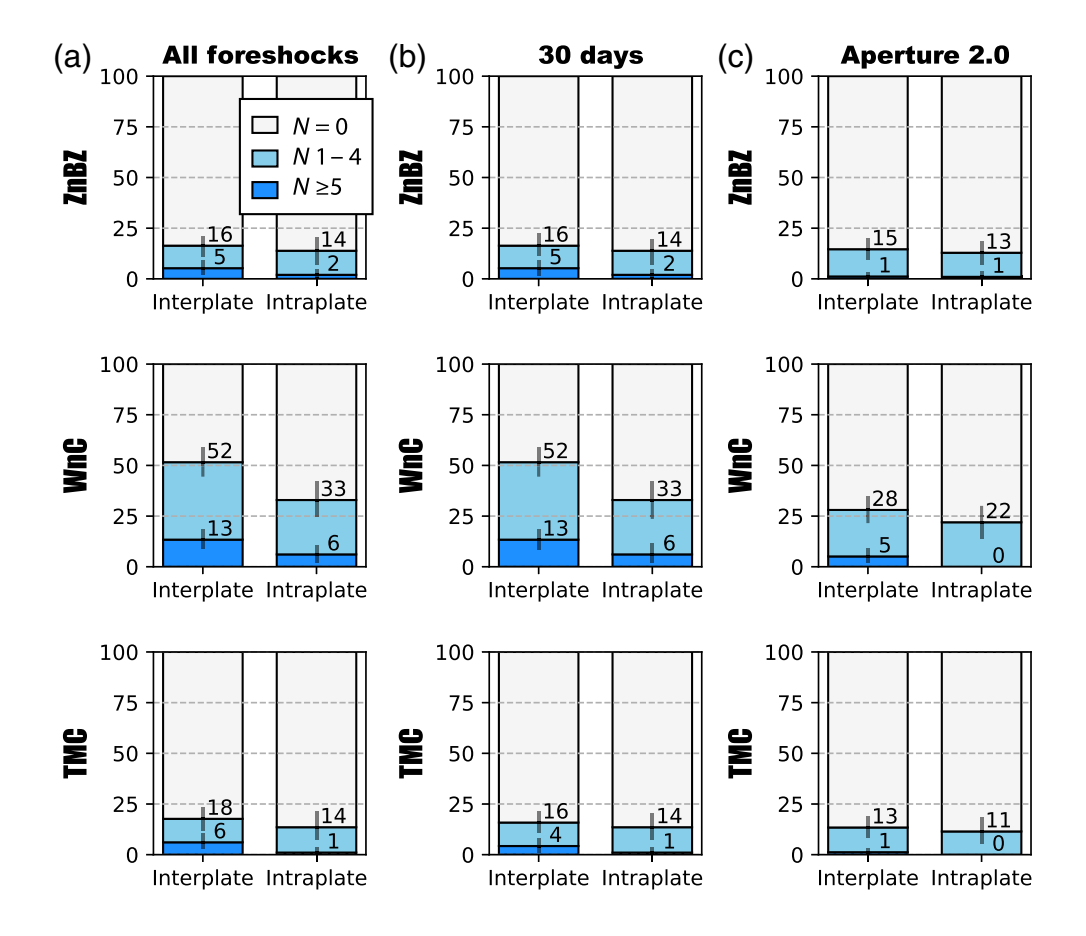


Figure 5. The percentage of interplate versus intraplate mainshock* events with foreshocks (colored portions of histograms, dark blue indicates the number of foreshocks ≥5, light blue indicates the number of foreshocks is from 1 to 4); the white portions indicate no foreshocks for the NEIC global catalog. This considers all earthquakes at and above the uniform completeness magnitude, $M_c = 5.0$ for the three clustering methods. The number of foreshocks is determined for three cases: (a) using all foreshocks in each individual cluster, (b) imposing a constant 30-day time window on all methods, and (c) considering only earthquakes within 2.0 magnitude units below the mainshock magnitude. The black vertical lines represent the 5% and 95% confidence level of 500 bootstrap random realizations of the populations. The color version of this figure is available only in the electronic edition.

heterogeneous stress conditions associated with sediments, fluids, and boundary topography than mature intraplate faults, accounting for this tendency. However, aftershock productivity levels have been reported to be higher for intraplate mainshocks than for interplate mainshocks in Japan (Yamanaka and Shimazaki, 1990), so regional variations are likely important.

We tested the relationship between the faulting geometry of the mainshock* obtained from the Global CMT catalog and the percentage of mainshocks with detectable foreshock activity for the three clustering algorithms for the NEIC global catalog. We find that foreshock activity is more common for reverse faulting mainshocks* compared with strike-slip and normal faulting (Fig. 6a). This trend becomes less clear after separation to interplate (Fig. 6b) and intraplate (Fig. 6c) mainshocks*. For interplate mainshocks* (Fig. 6b), normal faulting is more

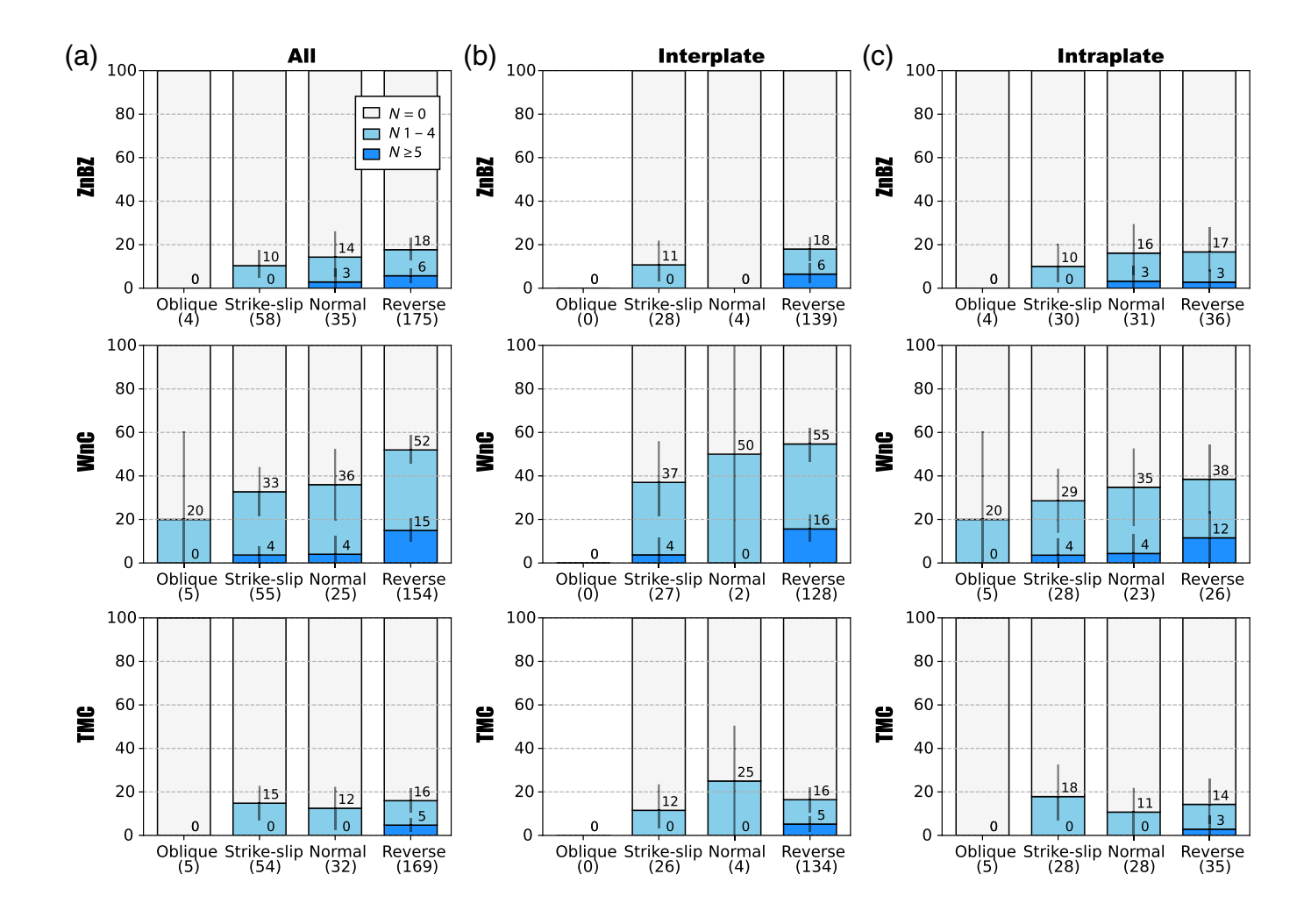
prone to have foreshock activity, but there are only few (4-6) cases of normal faulting, so this has low statistical significance. For the population of intraplate mainshocks*, the tendency of reverse mainshock* faulting to be preceded by foreshock activity is again slightly higher than for strike-slip and normal faulting mainshocks (Fig. 6c). These differences are subtle and vary with clustering procedure. Previous studies of global foreshock patters have recognized similar tendencies with foreshock being relatively higher before thrust events (largely associated with subduction zones) events and lower for strike-slip events (Reasenberg, 1999).

The Global CMT focal mechanisms for foreshock and aftershock events from the NEIC catalog are compared with the mainshock faulting geometry. Events having focal mechanism solutions with pressure, tension, and null axes all within 30° of the mainshock values are identified as "similar" events, and events with larger difference are defined as "different" (Fig. 7).

When considering all the detected sequences, the ZnBZ

(Fig. 7a), WnC (Fig. S9a), and TMC (Fig. S10a) show higher percentages of "similar" rather than "different" foreshocks. Comparison of the similarity of foreshocks and aftershocks with the mainshock according to three main faulting geometries—strike-slip (Fig. 7b), normal faults (Fig. 7e), and thrusts (Fig. 7f)—shows that for thrusts, there is higher percentage of similar foreshocks (72%) and aftershocks (65%). This feature is consistent for the WnC (Fig. S9a–d) and TMC (Fig. S10a–d) sequences. Strike-slip and normal mainshocks have more diverse foreshock mechanisms for WnC (Fig. S9b,c), but the populations are small, and such a trend is not evident for ZnBZ.

Further information is obtained when we classify interplate thrust events by the hypocentral depth to three domains following Lay *et al.* (2012). Foreshocks have more similar mechanisms for domains A (<15 km deep) for WnC and TWC but not for ZnBZ (Fig. 7c and Figs. S9e and S10e) and for all



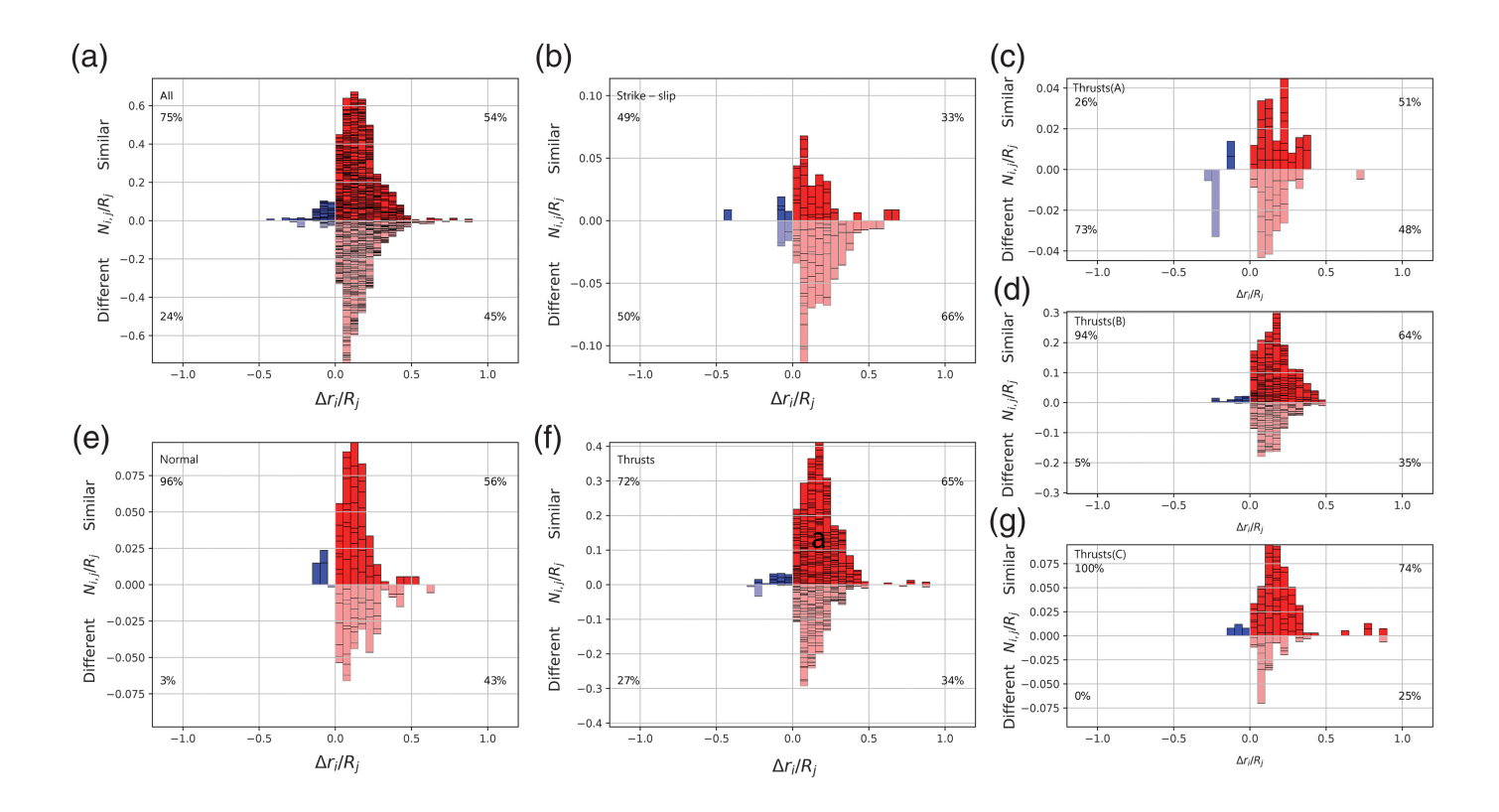
methods for domains B (15–35 km deep; Fig. 7d and Figs. S9f and S10f) and C (>35 km deep; Fig. 7g and Figs. S9g and S10g). Aftershocks have lower percentage of different mechanisms for domains B and C compared with domain A for ZnBZ (Fig. 7d, g), WnC (Fig. S9f,g) and TMS (Fig. S10f,g). The latter behavior is consistent with the findings for early aftershocks within the first two weeks after megathrust mainshocks (Wetzler et al., 2018).

Focusing on mainshock* events distributed around the circum-Pacific having ≥1 foreshock within 2.0 magnitude units below the mainshock magnitude (Fig. 3c), we detect regions that tend to lack observed foreshocks (albeit with scatter between methods), including South America, Mexico, New Zealand (Alpine fault), and the Philippines (note the paucity of blue-filled symbols in Fig. 8). Regions such Vanuatu, Solomon Islands, west Aleutians, and the Kuril Islands show higher percentages of events with foreshock activity.

Comparing interplate thrusting mainshock*, the western circum-Pacific tends to have a higher percentage of events with foreshock activity (Fig. 8). This observation is consistent for the three clustering algorithms, with +7%, +17%, and +2% increased occurrence of observable foreshocks detected for the ZnBZ, WnC, and TMC methods, respectively. The increase in

Figure 6. The percentage of foreshock occurrence for the NEIC catalog using the nearest-neighborhood algorithm (ZnBZ), magnitude-varying space + fixed-time windowing procedure (WnC), and time magnitude clustering (TMC) methods, considering the mainshock faulting geometry, classified for (a) all faulting types, (b) interplate mainshocks*, and (c) intraplate mainshocks*. The bars are colored for three levels based on the number of foreshocks as in Figure 3. The total number of each faulting type is plotted on the horizontal axes. The black vertical lines represent the 5% and 95% confidence level of 500 bootstrap random realizations of the populations. The color version of this figure is available only in the electronic edition.

foreshock activity is consistent with higher aftershock counts detected in the western circum-Pacific (Singh and Suárez, 1988; Wetzler et al., 2016). It has been proposed that the relative productivity level is associated with the thermal conditions of the subducting plate, producing more aftershocks for relatively older subducted oceanic plates (Dascher-Cousineau et al., 2020), but there is also a bimodal distribution of island arc subduction zones in the western Pacific and continental subduction zones in the eastern Pacific, so the



thermal and petrological properties of the upper plate may have an important influence.

Conclusions

General characteristics of global foreshock activity are studied based on the NEIC catalog combined with focal mechanism information obtained from the Global CMT catalog for all earthquakes of $M \ge 5$ and depth ≤ 70 km with mainshock magnitudes ≥7.0. Foreshock and aftershock sequences are defined by three clustering methods, focusing specifically on conventional mainshock-type sequences. For a magnitude aperture of 2, the percentages of mainshocks with observable foreshocks using two clustering methods based on earthquake-to-earthquake triggering that should suppress background activity, ZnBZ and TMC, are 14% and 13%, respectively; the WnC method, with a fixed time window of 30 days, has 26%. The results are generally consistent with prior estimates but depend on the method as previously found for regional catalogs, and no one method is unambiguously optimal. Although WnC method can overestimate foreshock numbers by capturing some background activity, the two linking methods may underestimate foreshock numbers caused by the sparseness of the seismicity for $M_c = 5.0$.

Each of the methods has advantages and disadvantages; although the ZnBZ method is more stringent and most likely to identify true foreshocks distinct from background, ZnBZ may miss many foreshocks if they are spatially and temporally less clustered, so counts of foreshocks may be biased low. But for methods that are more vulnerable to contamination by background, counts of foreshocks may be biased high. When

Figure 7. Composite scaled number of $(N_{i,j})$ of foreshocks (blue) and aftershocks (red) in the NEIC catalog with $M_{\rm w} \ge 5.0$ at scaled range of distances from the mainshocks epicenter (Δr_i) for sequences from the ZnBZ method for (a) all mainshocks*, (b) strike-slip mainshocks*, (e) normal-faulting mainshocks*, and (f) thrust-faulting mainshocks*. The individual distances (Δr_i) and earthquake counts $(N_{i,i})$ are normalized by the rupture length (R_i) of the mainshock (equation 1). The thrust subset for subduction zones is classified into three groups by mainshock hypocentral depth to (c) domain "A", depth <15 km, (d) domain "B" with 15 ≤depth <35 km, and (g) domain "C" with depth ≥35 km. Positive bars represent aftershocks and foreshocks with similar faulting geometry to the mainshock and negative bars represent events that are different from the mainshock's faulting geometry. The percentages of each subset (similar and different) from the entire foreshock or aftershock populations are plotted at each corner.

a catalog has low completeness level, as is the case for regional catalogs (for which $M_{\rm c}$ is usually as low as 3 and in special cases may go down to 1 or so), there are many events to create space–time links, even while there are likely many more background events. Then ZnBZ is likely superior for establishing dependencies on various parameters. However, for the global catalogs, the $M_{\rm c}$ of ~5 greatly reduces the number of events that can create space–time links, and for a short interval of time (30 days captures most sequences for the three methods), background rates of occurrence of M 5+ events is always low, so ZnBZ and TMC may have more bias toward lower foreshock counts than WnC, which is biased toward higher counts. We present the results for all three methods, recognizing the competing advantages and disadvantages so readers can consider the uncertainty in relationships.

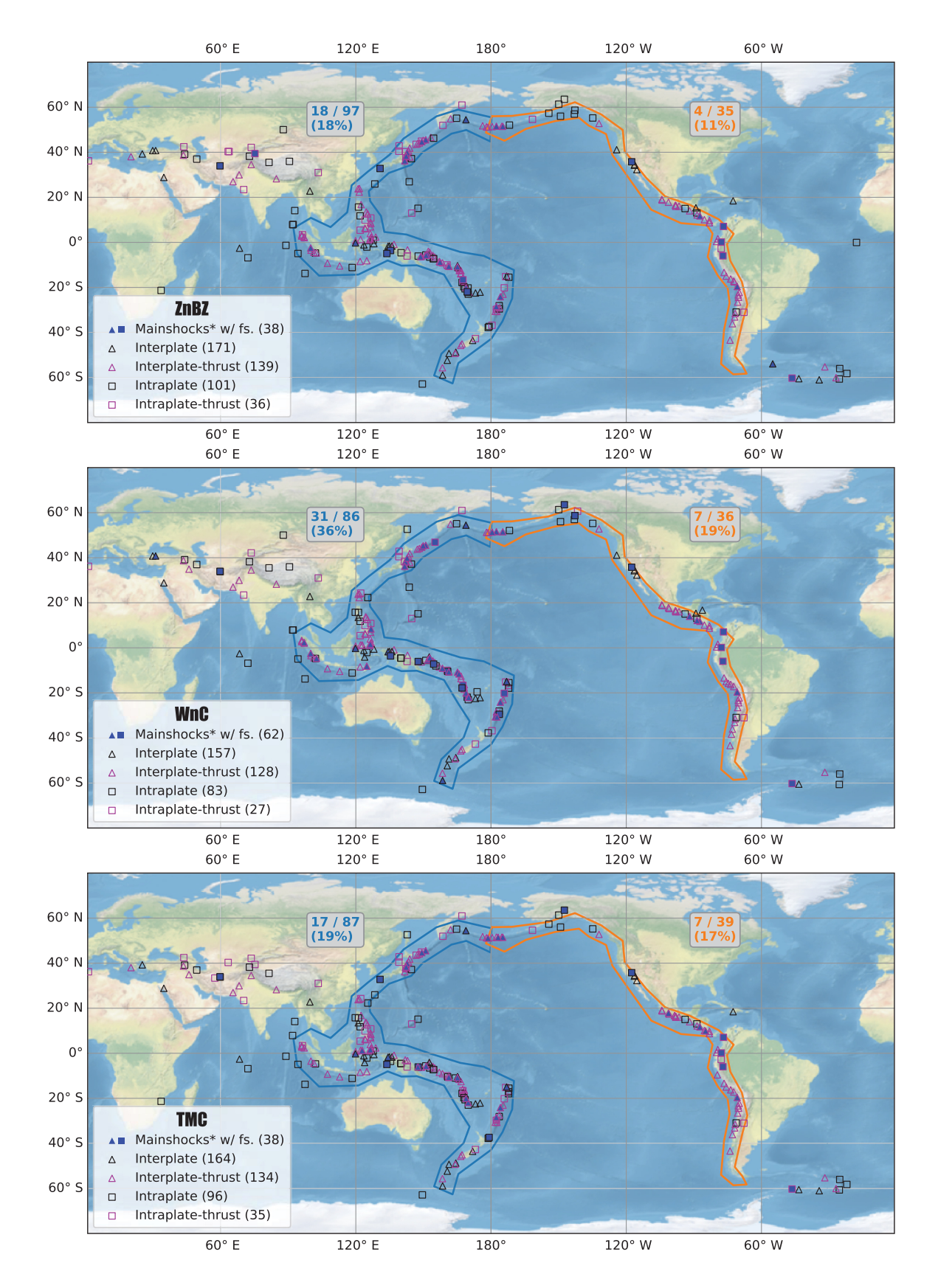


Figure 8. Designated mainshocks* for each clustering method, from the NEIC catalog having 1 or more foreshocks within 2.0 magnitude units below the mainshock* magnitude (Fig. 3c) are plotted by the blue-filled symbols on the map. Interplate (triangles), interplate-thrust (magenta triangles), intraplate (squares) and intraplate-thrust (magenta squares) mainshocks* are plotted

with the number of mainshocks* of each population shown in the legend. The fraction and percentage of events with foreshocks among interplate-thrust mainshocks* in the eastern Pacific (orange polygon) and the western Pacific (blue polygon) are shown at the top corners of each panel.

www.srl-online.org • Volume 94 • Number 5 • September 2023

The Gutenberg–Richter magnitude relationships for composite foreshock and aftershock sequences have lower *b*-value for foreshocks compared with aftershocks when including the entire foreshock sequence. The global trend in composite *b*-values is similar to the regional scale trend reported by Wetzler *et al.* (2022). However, when including only foreshocks between the largest foreshock and the mainshock, similar *b*-values are found for global foreshocks and aftershocks, whereas the regional study still found lower *b*-values in most well-resolved cases, so the composite global behavior may obscure some regional tendencies.

Our consideration of ETAS models (Fig. S7) also indicates a tendency to estimate lower b-values (relative to aftershocks) when considering the entire composite foreshock sequence for the three clustering methods and more comparable values when only foreshocks after the largest foreshock are considered. Petrillo and Lippiello (2021) found a corresponding tendency to measure lower b-values for foreshocks with magnitudes as low as 2 for their ETAS computations for mainshocks with magnitudes from 4 to 5. Seif et al. (2019) examine ETAS models with M_c 2.5–4. These low M_c catalogs, like our prior work on regional ETAS catalogs, provide superior sampling of the distributions for nearest-neighbor (and space-time window) clustering approaches (although the spatial distribution assumptions imposed in all ETAS models intrinsically introduce interactions with the clustering parameters). Thus, it is plausible that the observed *b*-value behavior is a result of application of space-time windowing and nearestneighbor clustering methods to a purely "cascade" sequence. So, it could be that the global sequences are on average dominated by cascade processes with any exceptions being obscured in the composite sequences. However, the application of space-time windowing methods to simulated catalogs is still intrinsically problematic because it depends on how the ETAS simulations distribute events spatially and what the properties of the space-time windows are.

There are many parameters in ETAS calculations and clustering algorithms, and the precise b-value behavior (and percentage of events with foreshocks) is difficult to exactly match because results vary with clustering method and choices of what events to retain in b-value estimation. The spatial distributions produced by parameters in simple ETAS are not intended to and do not closely approximate the actual spatial distributions of data (for example, see Fig. S7a), so applications of space-time clustering algorithms will deviate between real data that are distributed anisotropically along fault systems versus the blobby clusters in simple ETAS models. We do not believe that strong conclusions should be made regarding the fundamental nature of foreshock sequences as end members of cascading versus driven manifestations based on the composite measurements for the large M_c event population considered here. Real sequences may vary in whether there are slow-slipdriven sequences mixed in with cascades with the eventcompositing procedure obscuring any distinctive behavior. Our opinion is that the possible existence of such driven sequences should be tested for using very complete individual, low M_c , relocated sequences with good geodetic deformation control.

Additional differences in foreshock occurrence are observed using the information from faulting mechanisms. For example, foreshocks are somewhat more common for interplate mainshocks* than with intraplate mainshocks* and among all sequences are more common for reverse-faulting mainshocks* than for normal-faulting and strike-slip faulting mainshocks*. Relative to aftershocks, foreshocks tend to have more similar faulting mechanisms to the mainshock for normal-faulting and thrust-faulting events and are less diverse in mechanism relative to the mainshock for interplate thrusts in the central and deeper part of the megathrust.

The percentages of mainshocks* with detected foreshocks located along the western circum-Pacific is 2%–17% points larger than the eastern circum-Pacific for the three clustering methods. The differences between the eastern and western circum-Pacific may be due to differences in age of the subducted plate and nature of the upper plate, as suggested in previous studies of aftershock productivity (Singh and Suárez, 1988; Wetzler *et al.*, 2016). Older plates are thicker and thus have a greater abundance of available faulted crust that can be involved in secondary earthquake sequences (Dascher-Cousineau *et al.*, 2020).

These systematics, although subtle, are pragmatically useful in guiding expectations of foreshock occurrence rates, including identifying the type of earthquakes most likely to have foreshocks. Interplate thrust earthquakes on the western Pacific Rim are most likely to have observable foreshocks at current global detection levels. In addition, some of the patterns found in the global data were previously identified in regional catalogs as noted earlier.

The findings that foreshock occurrence and aftershock productivity are higher around the western Pacific than the eastern Pacific and that reverse-faulting events have higher foreshock and aftershock productivity than strike-slip events (Dascher-Cousineau *et al.*, 2020; Wetzler *et al.*, 2016) suggest that foreshock and aftershock generation are linked. One possibility is that both kinds of productivity are controlled by the abundance of available peripheral faults or a critical stress and strength state necessary for cascades to occur.

This correspondence is an important clue to the nature of foreshocks that needs to be fully incorporated into any successful explanation. In addition, there is an operational use to the observation. One can plan on using foreshocks more vigorously as a forecasting tool in which aftershock activity is high.

Data and Resources

The global earthquake data are from the U.S. Geological Survey National Earthquake Information Center catalog available at https://

earthquake.usgs.gov/earthquakes/search (last accessed October 2022). Focal mechanism information is obtained from the Global Centroid Moment Tensor catalog available at https://www.globalcmt.org/ CMTsearch.html (last accessed September 2021). The time magnitude clustering algorithm is available at https://github.com/nadavwetzler/ TMC (last accessed October 2022). The workflow and detailed explanations of the nearest-neighbor clustering method by Zaliapin and Ben-Zion (2013) are available at https://github.com/tgoebel/clusteringanalysis (last accessed June 2021). Omori-law fitting was done with python code available at https://github.com/tgoebel/aftershocks (last accessed November 2022). Maps are plotted by the Cartopy Python package available at https://scitools.org.uk/cartopy (last accessed October 2022). Code for calculating the Gutenberg-Richter magnitude distribution is available at https://github.com/nadavwetzler/b-value (last accessed December 2022). The ETAS Python code is available at https://github.com/lmizrahi/etas (last accessed May 2023). The supplemental material includes five figures and figure bundle S1 available at https://figshare.com/articles/figure/Figure_Bundle_S1/21511455 (last accessed November 2022).

Declaration of Competing Interests

The authors acknowledge that there are no conflicts of interest recorded.

Acknowledgments

The authors thank two anonymous reviewers for their helpful comments and suggestions. This research was supported by Grant Number 2017683 from the United States–Israel Binational Science Foundation (BSF) and by the Department of Energy (DOE) Basic Energy Science Program Grant Numbers 0000242877 and EAR-1761987 from the U.S. National Science Foundation (NSF). T. Lay's research on earthquake processes is supported by U.S. NSF Grant Number EAR-1802364. N. Wetzler's research on earthquake triggering is supported by the Israeli Science Foundation number 363/20.

References

- Baiesi, M., and M. Paczuski (2004). Scale-free networks of earthquakes and aftershocks, *Phys. Rev. E* **69**, no. 6, 066106, doi: 10.1103/PhysRevE.69.066106.
- Båth, M. (1965). Lateral inhomogeneities of the upper mantle, *Tectonophysics* **2**, no. 6, 483–514, doi: 10.1016/0040-1951(65)90003-X.
- Bird, P. (2003). An updated digital model of plate boundaries, *Geochem. Geophys. Geosys.* **4**, no. 3, doi: 10.1029/2001GC000252.
- Brodsky, E. E., and T. Lay (2014). Recognizing foreshocks from the 1 April 2014 Chile earthquake, *Science* **344**, no. 6185, 700–702, doi: 10.1126/science.1255202.
- Choy, G. L., and J. W. Dewey (1988). Rupture process of an extended earthquake sequence: Teleseismic analysis of the Chilean earthquake of March 3, 1985, *J. Geophys. Res.* **93,** no. B2, 1103, doi: 10.1029/JB093iB02p01103.
- Dascher-Cousineau, K., E. E. Brodsky, T. Lay, and T. H. W. Goebel (2020). What controls variations in aftershock productivity? *J. Geophys. Res.* **125,** no. 2, 1–18, doi: 10.1029/2019JB018111.
- Dziewoński, A. M., T.-A. Chou, and J. H. Woodhouse (1981). Determination of earthquake source parameters from waveform data for studies of global and regional seismicity *J. Geophys. Res.* **86**, no. B4, 2825–2852, doi: 10.1029/JB086iB04p02825.

- Ekström, G., M. Nettles, and A. M. Dziewoński (2012). The global CMT project 2004–2010: Centroid-moment tensors for 13,017 earthquakes *Phys. Earth Planet. Inter.* **200–201**, 1–9, doi: 10.1016/j.pepi.2012.04.002.
- Felzer, K. R., R. E. Abercrombie, and G. Ekstrom (2004). A common origin for aftershocks, foreshocks, and multiplets *Bull. Seismol. Soc. Am.* **94**, no. 1, 88–98, doi: 10.1785/0120030069.
- Gardner, J. K., and L. Knopoff (1974). Is the sequence of earthquakes in Southern California, with aftershocks removes, Poissonian? *Bull. Seismol. Soc. Am.* 64, no. 5, 1363–1367.
- Goebel, T. H. W., G. Kwiatek, T. W. Becker, E. E. Brodsky, and G. Dresen (2017). What allows seismic events to grow big?: Insights from b-value and fault roughness analysis in laboratory stick-slip experiments, *Geology* 45, no. 9, 815–818, doi: 10.1130/G39147.1.
- Gulia, L., and S. Wiemer (2019). Real-time discrimination of earth-quake foreshocks and aftershocks *Nature* **574**, no. 7777, 193–199, doi: 10.1038/s41586-019-1606-4.
- Hasegawa, A., K. Yoshida, Y. Asano, T. Okada, T. Iinuma, and Y. Ito (2012). Change in stress field after the 2011 great Tohoku-Oki earthquake, *Earth Planet. Sci. Lett.* **355–356**, no. B1, 231–243, doi: 10.1016/j.epsl.2012.08.042.
- Helmstetter, A., D. Sornette, and J.-R. Grasso (2003). Mainshocks are aftershocks of conditional foreshocks: How do foreshock statistical properties emerge from aftershock laws, *J. Geophys. Res.* **108**, no. B1, 1–24, doi: 10.1029/2002jb001991.
- Jones, L. M., and P. Molnar (1979). Some characteristics of foreshocks and their possible relationship to earthquake prediction and premonitory slip on faults, *J. Geophys. Res.* 84, no. B7, 3596–3608, doi: 10.1029/JB084iB07p03596.
- Kagan, Y., and L. Knopoff (1978). Statistical study of the occurrence of shallow earthquakes, *Geophys. J. Int.* **55**, no. 1, 67–86, doi: 10.1111/j.1365-246X.1978.tb04748.x.
- Kato, A., and T. Igarashi (2012). Regional extent of the large coseismic slip zone of the 2011 Mw 9.0 Tohoku-Oki earthquake delineated by on-fault aftershocks, *Geophys. Res. Lett.* 39, no. 15, 2–7, doi: 10.1029/2012GL052220.
- Lay, T., and H. Kanamori (1980). Earthquake doublets in the Solomon Islands, *Phys. Earth Planet. In.* **21**, no. 4, 283–304, doi: 10.1016/0031-9201(80)90134-X.
- Lay, T., H. Kanamori, C. J. Ammon, K. D. Koper, A. R. Hutko, L. Ye, H. Yue, and T. M. Rushing (2012). Depth-varying rupture properties of subduction zone megathrust faults, *J. Geophys. Res.* 117, no. B4, 1–21, doi: 10.1029/2011JB009133.
- Marsan, D., A. Helmstetter, M. Bouchon, and P. Dublanchet (2014). Foreshock activity related to enhanced aftershock production, *Geophys. Res. Lett.* **41**, no. 19, 6652–6658, doi: 10.1002/2014GL061219.
- Masse, R. P., and R. E. Needham (1989). NEIC the National Earthquake Information Center, *Earthquakes & Volcanoes* (USGS) **21**, no. 1, 4–44.
- McGuire, J. J., M. S. Boettcher, and T. H. Jordan (2005). Foreshock sequences and short-term earthquake predictability on East Pacific Rise transform faults, *Nature* **435**, no. 7041, 528–528, doi: 10.1038/nature03621.
- Mizrahi, L., S. Nandan, and S. Wiemer (2021). The effect of declustering on the size distribution of mainshocks, *Seismol. Res. Lett.* **92**, no. 4, 2333–2342, doi: 10.1785/0220200231.

- Mogi, K. (1963). Some discussions on aftershocks, foreshocks and earthquake swarms the fracture of a semi-infinite body caused by an inner stress origin and its relation to the earthquake phenomena, *Bull. Earthq. Res. Inst. Univ. Tokyo*, **41**, no. 3, 615–658.
- Moutote, L., D. Marsan, O. Lengliné, and Z. Duputel (2021). Rare occurrences of non-cascading foreshock activity in southern California, *Geophys. Res. Lett.* **48**, no. 7, doi: 10.1029/2020GL091757.
- Petrillo, G., and E. Lippiello (2021). Testing of the foreshock hypothesis within an epidemic like description of seismicity, *Geophys. J. Int.* **225**, 1236–1257, doi: 10.1093/gji/ggaa611.
- Reasenberg, P. A. (1999). Foreshock occurrence before large earthquakes, J. Geophys. Res. 104, no. B3, 4755–4768, doi: 10.1029/1998jb900089.
- Ruiz, S., M. Metois, A. Fuenzalida, J. Ruiz, F. Leyton, R. Grandin, C. Vigny, R. Madariaga, and J. Campos (2014). Intense foreshocks and a slow slip event preceded the 2014 Iquique M_w 8.1 earthquake, *Science* 6201, 1165–1169, doi: 10.1126/science.1256074.
- Seif, S., J. D. Zechar, A. Mignan, S. Nandan, and S. Wiemer (2019).
 Foreshocks and their potential deviation from general seismicity,
 Bull. Seismol. Soc. Am. 109, 1–18, doi: 10.1785/0120170188.
- Shearer, P. M., G. A. Prieto, and E. Hauksson (2006). Comprehensive analysis of earthquake source spectra in southern California, *J. Geophys. Res.* **111,** no. 6, 1–21, doi: 10.1029/2005JB003979.
- Singh, S. K., and G. Suárez (1988). Regional variation in the number of aftershocks (mb ⋈ 5) of large, subduction-zone earthquakes (Mw ⋈ 7.0), *Bull. Seismol. Soc. Am.* **78**, no. 1, 230–242.
- Tamaribuchi, K., Y. Yagi, B. Enescu, and S. Hirano (2018). Characteristics of foreshock activity inferred from the JMA earthquake catalog, *Earth Planets Space* **70**, 90, doi: 10.1186/s40623-018-0866-9.
- Trugman, D. T., and Z. E. Ross (2019). Pervasive foreshock activity across southern California, *Geophys. Res. Lett.* **46**, no. 15, 8772–8781, doi: 10.1029/2019GL083725.
- van den Ende, M. P. A., and J. P. Ampuero (2020). On the statistical significance of foreshock sequences in southern California, *Geophys. Res. Lett.* **47**, no. 3, 1–9, doi: 10.1029/2019GL086224.
- von Seggern, D., S. S. Alexander, and C.-E. Baag (1981). Seismicity parameters preceding moderate to major earthquakes, J.

- *Geophys. Res.* **86,** no. B10, 9325–9351, doi: 10.1029/JB086iB10p09325.
- Wells, D. L., and K. J. Coppersmith (1994). New empirical relationships among magnitude, rupture length, rupture width, rupture area, and surface displacement, *Bull. Seismol. Soc. Am.* 84, no. 4, 974–1002.
- Wetzler, N., E. E. Brodsky, E. J. Chaves, T. Goebel, and T. Lay (2022). Regional characteristics of observable foreshocks, *Seismol. Res. Lett.* doi: 10.1785/0220220122.
- Wetzler, N., E. E. Brodsky, and T. Lay (2016). Regional and stress drop effects on aftershock productivity of large megathrust earthquakes, *Geophys. Res. Lett.* 43, no. 23, 12,012–12,020, doi: 10.1002/ 2016GL071104.
- Wetzler, N., T. Lay, E. E. Brodsky, and H. Kanamori (2017). Rupture-depth-varying seismicity patterns for major and great ($M_{\rm w} \geq 7.0$) megathrust earthquakes, *Geophys. Res. Lett.* **44**, no. 19, 9663–9671, doi: 10.1002/2017GL074573.
- Wetzler, N., T. Lay, E. E. Brodsky, and H. Kanamori (2018). Systematic deficiency of aftershocks in areas of high coseismic slip for large subduction zone earthquakes, *Sci. Adv.* **4**, no. 2, 1–10, doi: 10.1126/sciadv.aao3225.
- Wilding, J. D., and Z. E. Ross (2022). Aftershock moment tensor scattering, *Geophys. Res. Lett.* **49**, no. 9, doi: 10.1029/2022GL098473.
- Yabe, S., and S. Ide (2018). Variations in precursory slip behavior resulting from frictional heterogeneity, *Progr. Earth Planet. Sci.*5, no. 1, doi: 10.1186/s40645-018-0201-x.
- Yamanaka, Y., and K. Shimazaki (1990). Scaling relationship between the number of aftershocks and the size of the main shock, *J. Phys. Earth* **38**, 305–324, doi: 10.4294/jpe1952.38.305.
- Zaliapin, I., and Y. Ben-Zion (2013). Earthquake clusters in southern California I: Identification and stability, *J. Geophys. Res.* **118**, no. 6, 2847–2864, doi: 10.1002/jgrb.50179.

Manuscript received 27 December 2022 Published online 28 June 2023